communications biology

A Nature Portfolio journal

Article

https://doi.org/10.1038/s42003-026-09586-y

Task demand modulates somatosensory-frontoparietal networks during delay and retrieval periods in tactile working memory

Dexin Sun [1,2,5], Jian Zhang[3,5], Shuyue Fu[3], Jingyuan Liu[1], Qing Liu[1], Shintaro Funahashi[1,3], Toshiya Murai[2], Jinglong Wu[1,3], Luyao Wang [4] ✉ & Zhilin Zhang [1,2] ✉

The primary somatosensory cortex (SI) is traditionally regarded as a sensory encoding region, yet growing evidence implicates it may also work in the maintenance and manipulation of tactile working memory (TWM), and interact with frontoparietal (FP) pathway under varying task demands. Here, we use high-field fMRI and a custom pneumatic tactile stimulation device to examine neural dynamics across distinct WM phases during a retro-cue task. We manipulate task demand during the delay phase (complex/simple retro-cues) and the retrieval phase (recall/non-recall) while isolating encoding, delay, and retrieval phases. Functional connectivity results reveal increased functional coupling between SI and FP regions as task demand increases. Moreover, effective connectivity results show the high-demand task selectively modulates excitatory connections from the posterior parietal cortex (PPC) to SI during maintenance, and from PPC to dorsolateral prefrontal cortex (dlPFC) as well as from dlPFC to SI during manipulation. These results demonstrate that SI engages in demand-dependent excitatory interactions with FP regions, supporting its central role throughout the whole TWM process.

Working memory (WM) is a short-term memory system that supports sensory encoding and temporary maintenance, enabling complex cognitive tasks across various types of sensory information[1]. WM capacity is constrained by finite neural resources and cognitive control mechanisms. Empirical studies[2,3] report that as task demand escalates (through greater information complexity or required manipulation), the WM system should allocate its limited neural resources more efficiently, resulting in characteristic capacity-precision trade-offs. Here, the frontoparietal (FP) network plays a central regulatory role, dynamically optimizing resource allocation through top-down control mechanisms, particularly by coordinating sensory cortical representations under high cognitive demands[4–6]. Extensive research has focused on visual and auditory WM; nevertheless, research on how tactile working memory (TWM) processes and retains somatosensory information remains comparatively limited.

Studies on TWM have identified a functional division across brain regions: the primary somatosensory cortex (SI) majorly responsible for encoding basic sensory information, and the FP network serves as a central hub for cognitive control and resource allocation[7]. This division mirrors findings in common WM research, where sensory areas encode stimulus features while FP regions, including the dorsolateral prefrontal cortex (dlPFC) and posterior parietal cortex (PPC), implement control processes. Contrary to the classical paradigm that relegates the SI to sensory encoding, converging evidence from non-human electrophysiology[8] and human neuroimaging now establishes its active participation in TWM maintenance, exhibiting task-demand-dependent activation profiles[9–11].

Crucially, perturbation studies show that the activation of SI is associated with the FP network dynamics during TWM processes, suggesting its underlying role in sensory storage[12,13]. Hypothetically, FP networks regulate sensory representations in somatosensory areas through top-down control, especially as task demands increase. Established evidence shows that distinct cognitive demands recruit differential connectivity patterns during various WM phases[14–16]. However, extant human functional magnetic resonance imaging (fMRI) investigations of TWM have significant limitations,

[1]Research Center for Medical Artificial Intelligence, Shenzhen Institute of Advanced Technology, Chinese Academy of Sciences, Shenzhen, Guangdong, China. [2]Department of Psychiatry, Graduate School of Medicine, Kyoto University, Kyoto, Japan. [3]School of Medical Technology, Beijing Institute of Technology, Beijing, China. [4]School of Life Sciences, Shanghai University, Shanghai, China. [5]These authors contributed equally: Dexin Sun, Jian Zhang.
✉e-mail: wangly1018@shu.edu.cn; zhangzhilin@siat.ac.cn

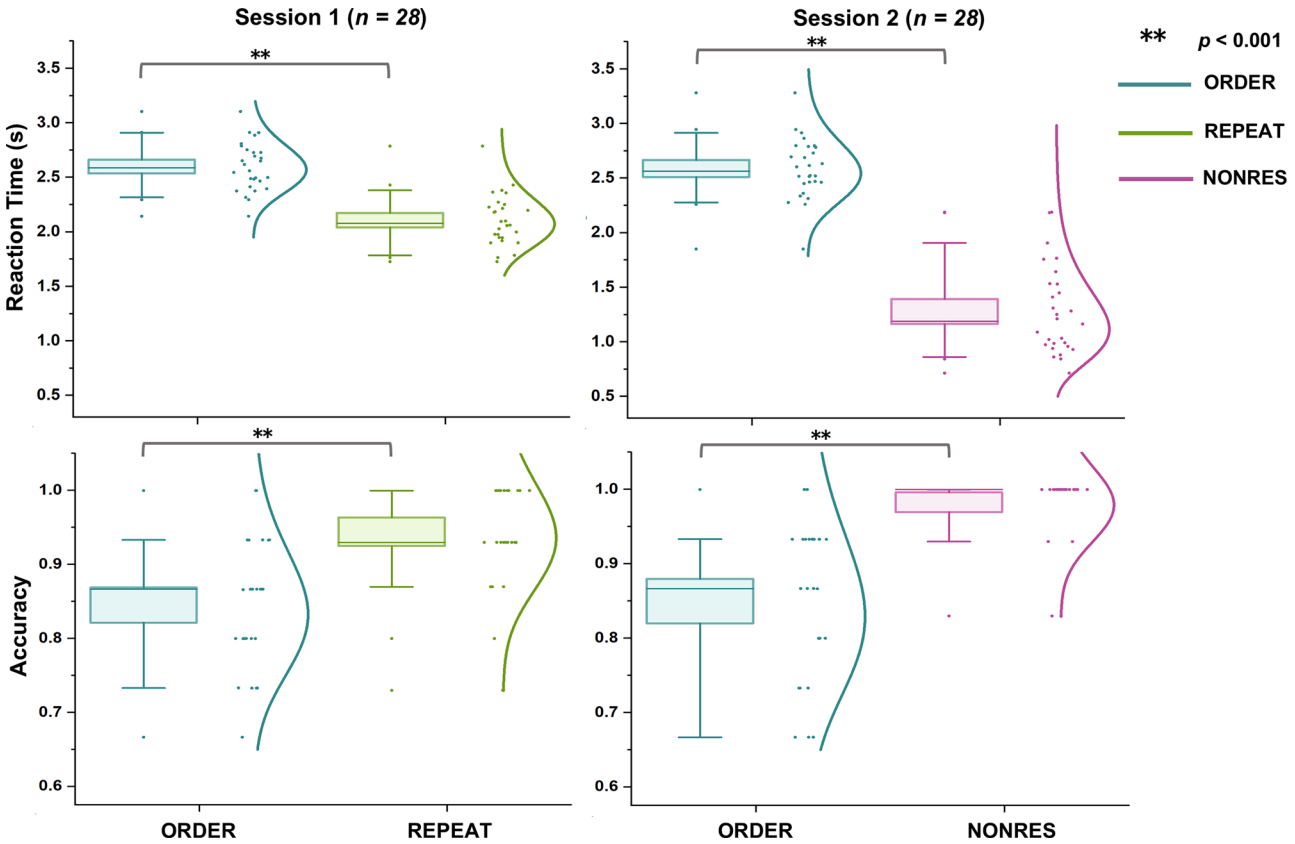

Fig. 1 | Behavioral performance (RT and accuracy) between the ORDER and REPEAT conditions in Session 1 and the ORDER and NONRES conditions in Session 2 (n = 28). The box range extends from mean−1.5×standard error (SE) to mean+1.5×SE, whereas the whiskers represent 10–90th percentiles of data distribution. Notably, the line on the right of the box shows the lognormal data distribution. Statistically significant differences are marked by asterisks: '**' $p < 0.001$.

primarily owing to dissociate phase-specific neural computations (encoding vs. delay vs. retrieval)[17]. This unresolved specificity obscures the mechanistic understanding of how SI and FP systems dynamically reconfigure their interactions in response to varying task demands.

To address this issue, a pneumatic-mechanical tactile stimulation device that can deliver precise vibrotactile stimulation to individual fingertips in a high-magnetic-field environment was developed. Our fMRI paradigm incorporates three distinct cognitive phases: tactile information encoding, delay, and retrieval. To investigate how task demand modulates neural processing during delay and retrieval phases, we used a carefully controlled retro-cue design[18,19]. First, we ensured that the tactile sensory input was identical during the encoding phase across all task conditions. Next, we manipulated task demands in the delay phase by providing either complex retro-cues (ORDER condition, high demand) or simple retro-cues (REPEAT condition, low demand). Finally, during retrieval, we further varied recall requirements by including both recall tasks (ORDER condition) and non-recall tasks (NONRES condition). This phase-specific demand manipulation allows for precise characterization of how neural networks dynamically adapt to varying demands at different stages of TWM processing.

In this study, we used a combination of psychophysiological interaction (PPI) analysis[20] and dynamic causal modeling (DCM) at the group level[21,22] to characterize how somatosensory-frontoparietal connectivity evolves during various TWM phases, especially during the delay and retrieval phases. We selected the left SI as a seed region of interest (ROI) owing to its direct input role in sensory. Two key nodes of the left FP network were also included as ROIs: the PPC and dlPFC, which are critically involved in higher-order cognitive control functions. Our neuroimaging findings provide compelling evidence that task demand modulates SI recruitment during delay and retrieval phases, while also enhancing its dynamic interaction with FP networks.

Results

Behavior performance

In TWM tasks, the paired samples t-test was used to test for differences in behavioral variables, including reaction time (RT) and accuracy (Fig. 1, Table 1, Supplementary Data 1). For the RT statistic, only trials with correct answers were included, while error trials were systematically excluded. The mean and standard deviation (SD) for each variable were calculated for the 28 participants in each condition, including 15 trials. Factors such as sex and years of education were not significantly associated with any of the behavioral variables. In Session 1, the ORDER condition compared with the REPEAT condition showed longer RTs (Mean ± SD; ORDER: 2.60 ± 0.22 s, REPEAT: 2.11 ± 0.19 s) and lower accuracy (Mean ± SD; ORDER: 0.84 ± 0.08, REPEAT: 0.94 ± 0.07). Similarly, in Session 2, the ORDER condition was associated with longer RTs (Mean ± SD; ORDER: 2.59 ± 0.27 s, NONRES: 1.28 ± 0.44 s) and lower accuracy (Mean ± SD; ORDER: 0.85 ± 0.08, NONRES: 0.98 ± 0.05) than the NONRES condition. These results show that the high-demand condition (ORDER) led to poorer behavioral performance than the low-demand condition (REPEAT/NONRES), highlighting a clear gradient of demand in our experiment.

Whole-brain activation

Statistical analyses were conducted using a standard GLM approach with SPM12. Incorrect trials were excluded, and regressors for encoding, delay, and retrieval phases across ORDER, REPEAT, and NONRES conditions were modeled at the first level. At the second level, conjunctions identified regions of general tactile processing, the contrast ORDER > REPEAT was

Table 1 | Cognitive ability scores and behavioral performance data of participants (N = 28)

Task	Description	Scores (SD)
	Sex(female/male)	15/13
	Age	24.9(1.8)
	Age range	23–29
	Education Year	18.32(1.07)
	MMSE	29.93(0.26)
	MOCA-B	29.61(0.77)
	SCD-Q24	23.03(1.57)
	AVLT	98(3.80)
	TMT (s)	57.27(9.32)
	SDMT	49.21(4.49)
ORDER	ACC	0.86(0.08)
	RT(s)	2.57(0.25)
REPEAT	ACC	0.94(0.07)
	RT(s)	2.11(0.23)
NONRES	ACC	0.98(0.05)
	RT(s)	1.28(0.40)

used to examine differential activations associated with increased task demands, whereas the contrast ORDER > NONRES specifically targeted brain regions involved in recall-related processes. We assessed group-level effects via a within-subjects ANOVA and reported results at a voxel-wise FWE-corrected threshold of $p < 0.05$.

The significant activations (Table 2) in the ORDER ∩ REPEAT ∩ NONRES contrast during the encoding period, the ORDER > REPEAT and ORDER ∩ REPEAT contrasts of Session 1 during the delay period, and the ORDER > NONRES and ORDER ∩ NONRES contrasts of Session 2 during the retrieval period were all analyzed. For all ROIs, we report the MNI coordinates of the peak voxel and its associated T-statistic. A significant co-activation of regions associated with tactile sensation in the left hemisphere was observed during the encoding phase. This included the SI, the post-central gyrus, the superior frontal gyrus, the supplementary motor area, the parietal gyrus, and the basal ganglia. However, during the delay period (Fig. 2B), all the regions of interest (ROIs: SI, PPC, and dlPFC) showed greater differential activation in the ORDER condition than in the REPEAT condition, as well as those that were co-activated in the ORDER and REPEAT conditions. During the retrieval period (Fig. 2C), ROIs were evoked in the ORDER and NONRES conditions. The ROIs showed enhanced activation in the ORDER condition compared to the NONRES condition. These results show that ORDER consistently elicited stronger activation in the left SI and FP regions compared with the low-demand tasks (REPEAT or NONRES). This suggests that the ROIs are highly recruited for encoding, maintaining, and manipulating tactile sensory information with increasing task demand. To visualize the condition-specific changes in beta values, we plotted the event-related average (ERA) curves for the left SI from a single trial (Fig. 3). This ERA curve represents the temporal dynamics of the SI's beta values and aligns with the whole-brain findings.

Functional connectivity

We selected the left SI (x = −44, y = −32, z = 46) as the seed region because it showed robust peak activation in the critical contrasts (ORDER > REPEAT during the delay period and ORDER > NONRES during the retrieval period), indicating its central role in both increased task demands and recall-related processes. Functional connectivity was observed with the frontoparietal regions, modulated by contrasts (Table 3). During the delay period (Fig. 4A), the functional connectivity between the SI seed and PPC (x = −26, y = −50, z = 38), and that between the SI seed and dlPFC (x = −20, y = 48, z = 36), was significantly enhanced in the ORDER > REPEAT contrast of Session 1. Figure 4B shows the significantly activated connection between the SI seed and PPC and that between the S1 seed and dlPFC in the ORDER > NONRES contrast of Session 2 during the retrieval period. These results show the positive activation of a functional network between the SI, dlPFC, and PPC during the delay and retrieval periods, reflecting the enhanced connections modulated by the increasing demand.

Table 2 | Group significant co-activation and differential activation in the whole brain during TWM, with a voxel-level threshold of FWE $p < 0.05$

Brain regions	T scores (peak-level)	Peak MNI Coordinates		
		x	y	z
Encoding period (ORDER ∩ REPEAT ∩ NONRES)				
L Precentral gyrus	11.38	−46	−22	60
L SMA	9.19	−8	12	54
L Superior temporal gyrus	9.43	−50	−36	22
L prefrontal gyrus	8.23	−52	6	36
L Superior parietal gyrus	6.98	−28	−10	52
R Motor Cortex	10.13	38	−22	58
Delay period – Session 1 (ORDER > REPEAT)				
L Postcentral gyrus	8.23	−50	−8	54
L Posterior parietal cortex	7.21	−28	−50	48
L PFC	6.32	−20	48	36
L SI	5.12	−44	−32	46
R Posterior parietal cortex	5.69	36	−48	50
R Precentral gyrus	4.95	50	−2	44
R PFC	3.98	44	32	26
(ORDER ∩ REPEAT)				
L PPC	9.23	−30	−56	46
L PFC	6.58	−20	42	38
L SI	5.31	−46	−32	42
L Inferior frontal gyrus	4.56	−46	14	30
R Superior parietal gyrus	8.29	36	−54	56
Retrieval period – Session 2 (ORDER > NONRES)				
L Postcentral gyrus	6.12	−50	−8	54
L PPC	10.12	−26	−52	44
L SI	5.56	−40	−32	40
L PFC	4.14	−20	46	30
R Middle frontal gyrus	8.60	30	16	56
R Inferior parietal gyrus	6.24	36	−52	48
(ORDER ∩ NONRES)				
L PPC	10.75	−34	−58	44
L PFC	9.98	−20	50	38
L SI	7.62	−42	−32	42
R PPC	8.25	50	−40	38
R Superior parietal lobule	6.48	10	−64	40

Effective connectivity

PEB analysis was used to evaluate the DCMs for the ORDER and REPEAT conditions during the delay period, as well as those for the ORDER and NONRES conditions during the retrieval period in Session 2. We calculated the connectivity parameters (Ep) and posterior model probabilities (Pp) values of the intrinsic and extrinsic connections (matrix A) and the modulatory connections (matrix B).

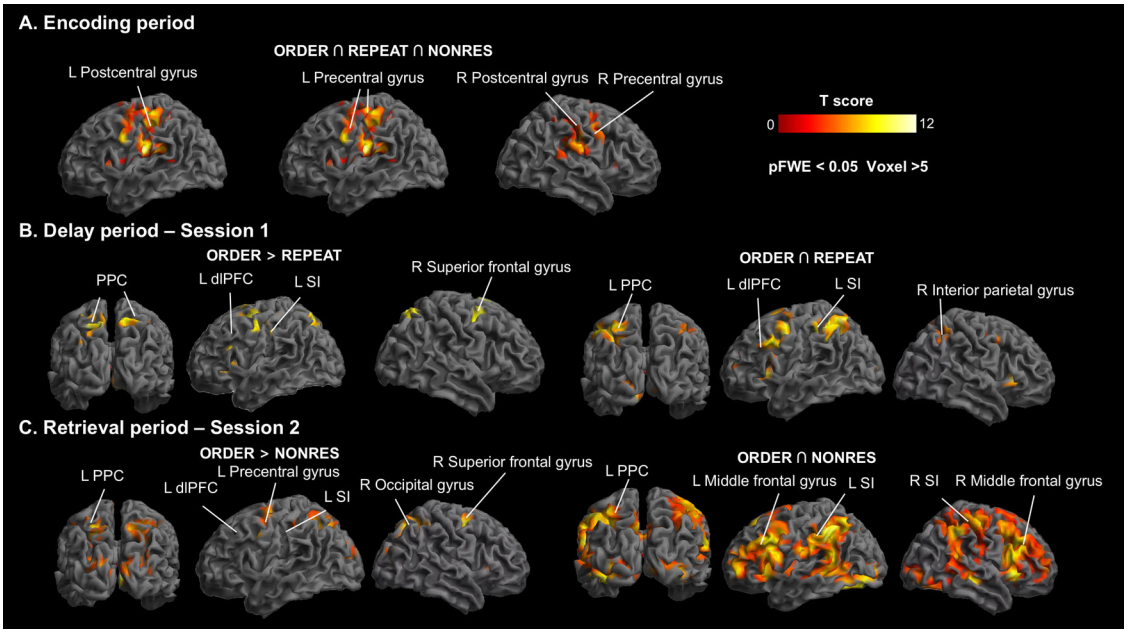

Fig. 2 | The whole-brain activation. A During the encoding period, the co-activated regions (the postcentral gyrus and precentral gyrus) of ORDER, REPEAT, and NONRES conditions. **B** During the delay period of Session 1, differentially activated regions in the ORDER > REPEAT contrast and co-activated regions of ORDER and REPEAT conditions. **C** During the retrieval period of Session 2, positive differentially activated regions in the ORDER > NONRES contrast and co-activated regions of ORDER and NONRES conditions. Notably, all regions were reported with a voxel-level threshold of FWE $p < 0.05$.

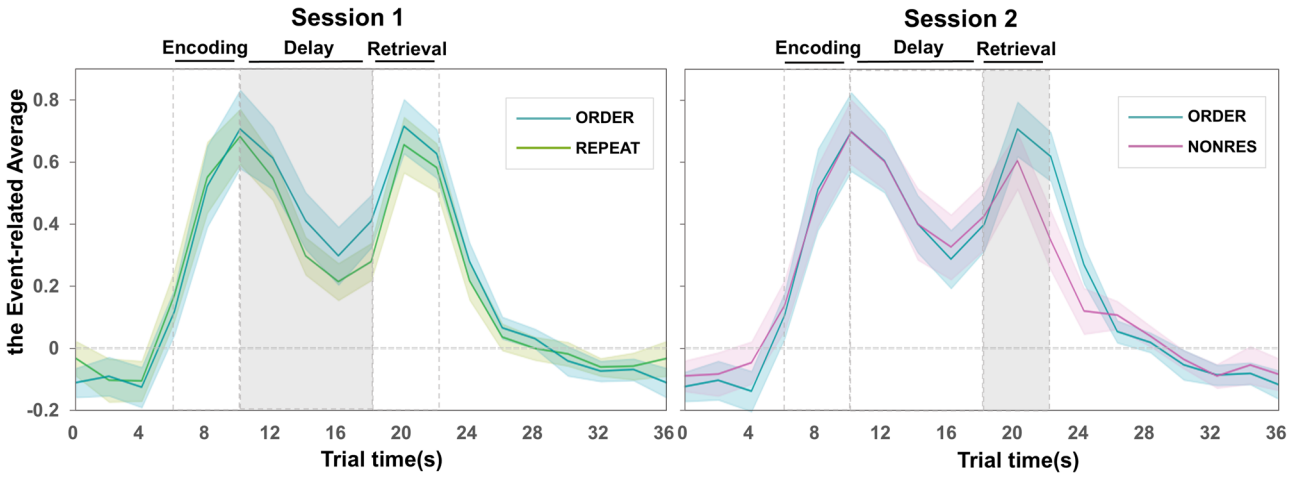

Fig. 3 | The illustrated curve of ERA in the left SI ($x = -44, y = -32, z = 46$) as the trial time (s) increases. The lines represent the mean, whereas the shaded areas indicate the 95% confidence intervals for the average (28 participants, 15 trials for each condition in a session).

Table 3 | Using the left SI as a seed point, group-level positive activations of ROIs during the delay period in Session 1 and the retrieval period in Session 2 were reported with a voxel-level threshold of FWE $p < 0.05$

Brain regions	T scores (peak-level)	Peak MNI Coordinates		
		x	y	z
Delay period – Session 1 (ORDER > REPEAT)				
L dlPFC	5.43	−20	48	36
L PPC	4.12	−26	−50	38
Retrieval period – Session 2 (ORDER > NONRES)				
L dlPFC	4.18	−20	46	34
L PPC	2.78	−24	−44	38

Table 4 shows the intrinsic and extrinsic connections (matrix A) between ROIs, including self-inhibitory and between-region connections. In Session 1, strong evidence showed that the average connections in the dlPFC → SI (Ep = −0.030) and PPC → dlPFC (Ep = −0.806) were anticorrelated, whereas the average connections in the SI → dlPFC (Ep=0.178), SI → PPC (Ep=0.464), and the dlPFC → PPC (Ep=0.264) were excitatory. The connections in the dlPFC → SI (Ep=0.567) and the PPC → dlPFC (Ep=0.079) were significant positive connections in session 2.

Table 5 shows the connection parameters (matrix B) in the SI-dlPFC-PPC network modulated by the demand difficulty. During the delay period (Fig. 5B.a) in Session 1, positive and stronger modulatory effects in the PPC → SI (ORDER: Ep=5.718, REPEAT: Ep=4.137) were observed in the ORDER condition than in the REPEAT condition. Although the dlPFC → SI (ORDER: Ep=0.548, REPEAT: Ep=0.984) pathway exhibited a certain degree of activation, it did not reach strong evidence (Pp < 0.95).

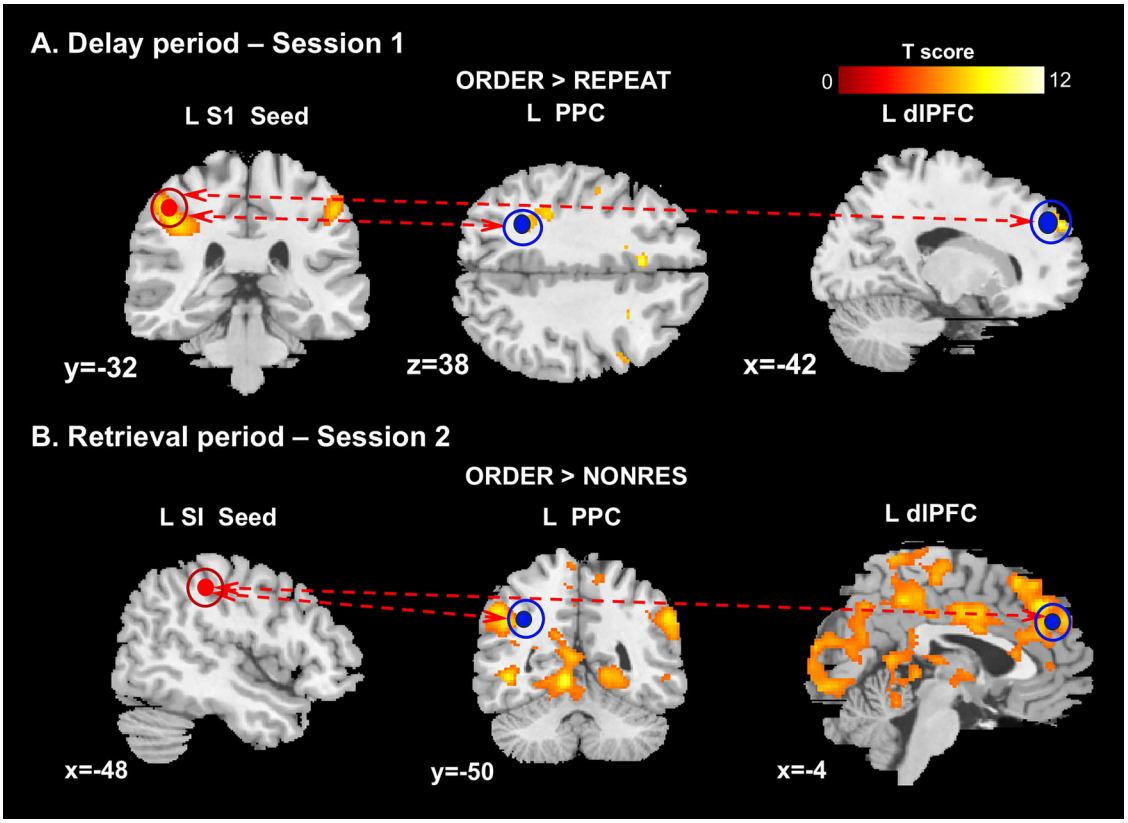

Fig. 4 | Functional connectivity using the left SI (x = −44, y = −32, z = 46) as the seed ROI. Connections in the left hemisphere between SI and PPC, as well as between SI and dlPFC, were strengthened for the ORDER > REPEAT contrast during the delay period in Session 1 (**A**) and for the ORDER > NONRES contrast during the retrieval period in Session 2 (**B**).

Table 4 | Ep and Pp values of intrinsic and extrinsic connections (matrix A) of group-average DCMs

To↓ From → (Ep/Pp)	Session 1			Session 2		
	SI	PPC	dlPFC	SI	PPC	dlPFC
SI	−1.092/1.00*	0.709/1.00*	−0.030/1.00*	−0.612/1.00*	0.005/0.88	0.567/1.00*
PPC	0.464/0.38	−0.706/1.00*	0.264/1.00*	0.045/0.05	−0.418/1.00*	0.144/0.99*
dlPFC	0.178/1.00*	−0.806/1.00*	−0.006/1.00*	0.237/0.81	0.079/1.00*	−0.502/1.00*

The asterisk symbol '*' indicates a significant connectivity with a Pp > 95%.

Additionally, a positive modulatory effect of the connection in the PPC → dlPFC (Ep=0.376, Pp=0.54) was observed in the ORDER condition. However, during the retrieval period (Fig. 5B.b) in Session 2, significant positive modulatory effects of the connection in the dlPFC → SI (Ep=1.552) and the PPC → dlPFC (Ep=1.785) and slight modulatory effects of the connection in the dlPFC → PPC (Ep=0.089) were observed in the ORDER condition. Furthermore, excitatory modulatory connections in the dlPFC → SI (Ep=0.498, Pp=0.9) were observed in the NONRES condition. Figure 5C shows the driving inputs to the SI node. The results of effective connectivity revealed that the high-demand condition elicited stronger dynamic interactions within the SI-frontoparietal network during the delay and retrieval periods. The excitatory connectivity, especially the PPC → SI pathways, is modulated by high task demand, emphasizing enhanced neural communication and coordination with increasing demand.

Discussion

In this study, the functional and effective connectivity between the SI and FP regions during TWM was investigated. First, the behavioral results indicated that conditions with high task demand resulted in poorer behavioral performance than those with low demand. Second, whole-brain imaging results provided evidence of significant activation within the SI-FP network as the task demand increased. Additionally, the observed signal changes in the left SI and its enhanced functional connections with FP regions modulated by higher demand elucidate its importance in coordinating the encoding, delay, and retrieval of TWM. Finally, the high-demand condition in the delay phase (ORDER condition) showed positive modulatory effects on the PPC → SI and the PPC → dlPFC connections. This study highlights the specific role of the SI in dynamically adapting to high-demand conditions by enhancing its connectivity and coordinating with the FP regions, especially during the delay and retrieval phases of TWM.

Behavioral performance

The behavioral results (Fig. 1, Table 1) showed significant differences in task reaction time and accuracy between the high- and low task demands, with task performance ranked as NONRES > REPEAT > ORDER. These significant differences in task performance across conditions indicate that our experimental design effectively differentiated the difficulty level of the task demand. The ORDER condition placed greater memory demands on participants. This reduced their performance compared with low-demand conditions, including REPEAT and NONRES. This aligns with studies on

WM demands, in which increased memory content requires greater WM capacity, while the capacity is often limited[23,24]. Therefore, a higher demand can result in a decline in behavioral performance.

Interaction between SI and FP regions in TWM process

The whole-brain analysis (Fig. 2) and ERA curve (Fig. 3) shows the increased activation of the left SI while maintaining and manipulating the various phases, corresponding to an increase in demand difficulty. This suggests the involvement of the SI, even when external stimuli are absent during the delay period, further emphasizing that the SI may actively contribute to memory processes beyond simple sensory encoding. Notably, this increase was predominantly observed in the left SI, contralateral to the stimulated hand, whereas the right SI exhibited only minimal or non-significant changes. Such hemispheric asymmetry argues against a purely domain-general interpretation based on task difficulty or arousal, which would be expected to engage bilateral sensory cortices more uniformly. Instead, the lateralized pattern implies that the contralateral SI retains stimulus-specific representations related to the tactile information maintained during the delay phase. This observation aligns with previous electrophysiological studies in primates[8,25–28], showing that SI neurons can sustain tactile information even without external stimulation, particularly under high memory demand. The activity change thus supports the view that the SI contributes to maintaining tactile representations under higher cognitive demands and facilitates appropriate responses instructed by tactile information[13].

At the same time, our experimental findings also reveal strong co-activation of the SI with the frontoparietal regions that belong to the Multiple Demand (MD) Network[29]. This pattern does not contradict the representational interpretation; rather, it suggests that domain-general control systems interact with modality-specific sensory regions to sustain relevant information under high-demand conditions. In the high-demand ORDER condition, enhanced activation within the SI–frontoparietal network indicates that top-down signals from the dlPFC and PPC may strengthen or modulate tactile representations in the contralateral SI. The dlPFC, the core of executive functions in WM, manages higher cognitive operations such as planning, decision-making, and manipulation of stimulus information[7,30,31], while the PPC supports spatial attention and sensory integration[6,32,33]. Evidence from macaque stimulation studies[34–36] likewise suggests that the dlPFC exerts temporally dependent top-down modulation on SI activity. Taken together, the contralateral dominance of SI activation and its functional coupling with the MD network point to a dynamic interaction in which top-down executive control enhances content-specific tactile representations maintained in SI during WM. Such lateralized yet coordinated activity patterns could be further examined through connectivity analyses[9,10].

Table 5 | Ep and Pp values of modulatory connections (matrix B) of group-average DCMs

Modulation (Ep/Pp)	Session 1		Session 2	
	ORDER	REPEAT	ORDER	NONRES
SI → PPC	-	-	-	-
SI → dlPFC	-	-	-	-
dlPFC → SI	0.548/0.78	0.984/0.90	1.552/1.00*	0.498/0.90
dlPFC → PPC	-	-	0.089/0.45	-
PPC → SI	5.718/1.00*	4.137/1.00*	-	
PPC → dlPFC	0.376/0.54	-	1.785/1.00*	-

The asterisk symbol '*' indicates a significant connectivity with Pp > 95%.

Functional connectivity between the SI and the FP pathway

The PPI results in Fig. 4 show significant connections between the SI and the FP pathway during the delay and retrieval periods, especially modulated by the higher demand condition. An electroencephalogram source reconstruction study[12] clarified that the sensory cortex mediates information storage by processing sensory signals. The SI encodes tactile stimuli when

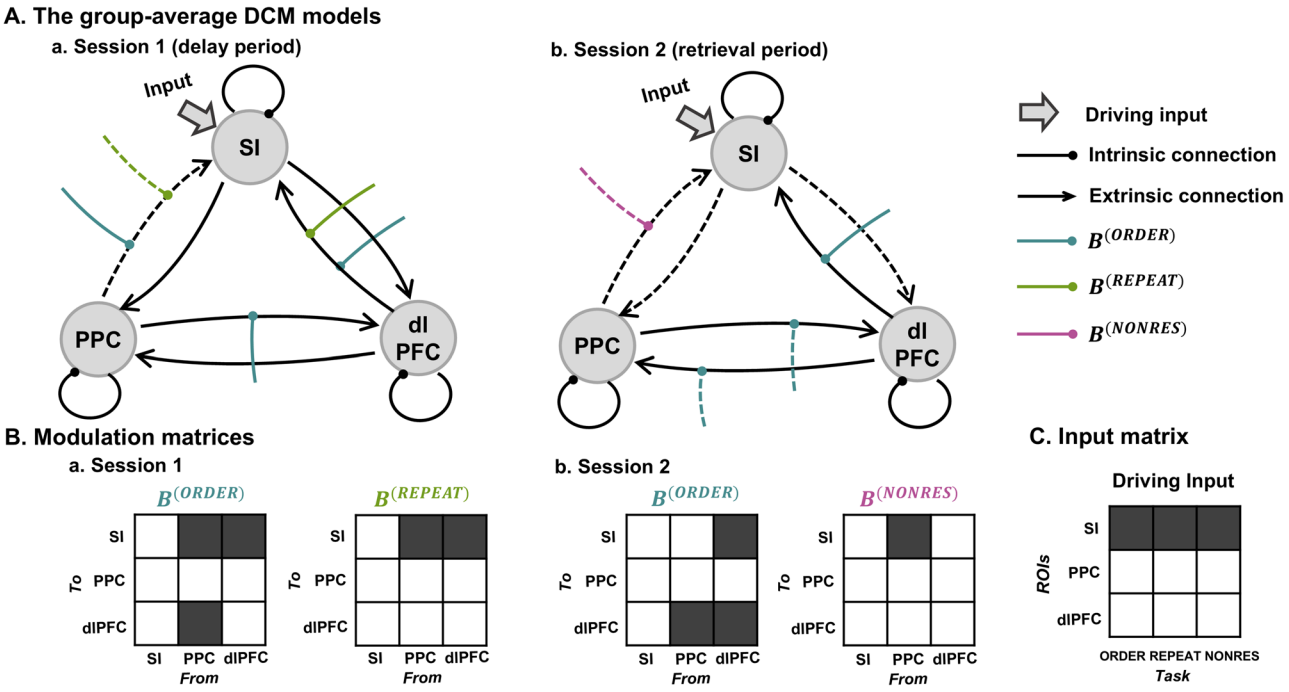

Fig. 5 | Group-average effective connections of DCM models with PEB analysis. **A** The group-average DCM models of the SI-dlPFC-PPC network in (A.a) Session 1 (ORDER vs. REPEAT) and (A.b) Session 2 (ORDER vs. NONRES), including intrinsic self-connections, extrinsic between-region connections, task-related driving inputs, modulatory connections by ORDER, REPEAT, and NONRES conditions. Solid lines represent significant connections with Pp > 0.95, whereas dashed lines represent non-significant connections. **B** Modulation matrices in (B.a) Session 1 and (B.b) Session 2 by WM tasks, corresponding to significant modulatory connections (black) and non-significant modulatory connections (white) between ROIs. **C** Driving input matrix in ORDER, REPEAT, and NONRES conditions.

they are perceived. They generate transient discharges, especially under low task demand conditions in the TWM, as shown in previous electrophysiological studies[13]. Specific regions in the somatosensory cortex (eg., BA1-3) are responsible for encoding and maintaining tactile stimuli during short-term storage[8,17]; therefore, the SI would be recruited more to cooperate with other cortical regions to manage increasing task demand. These results support the compensatory neural mechanism in TWM[37–39], where the SI requires closer association with other cortical regions to manage higher demand. This association helps to maintain signal transformation and continuity across the sensory cortex.

The SI is activated under high and low memory demands; however, stronger activation and connectivity in high-demand conditions emphasize its cooperative role with the frontoparietal regions in managing memory information. This strengthened connectivity highlights the need for the brain to recruit additional neural networks, especially those involved in memory and attention, to effectively manage and process the difficulty of increased demand. This synchronization pattern shows that the SI and PPC coordinate more closely with an increased memory demand.

Moreover, a study on visual and auditory WM has shown that the dorsal FP attention network encodes spatial information in a supramodal manner[40]. This finding suggests that information from different sensory modalities is represented by a shared neural code in these regions, rather than by modality-specific patterns. Such supramodal coding may similarly underpin TWM representations, with the FP network integrating inputs across multiple modalities to form unified cognitive representations. Overall, the functional results provide strong evidence for a demand-dependent compensatory mechanism[41], wherein the SI enhances its connectivity with FP regions, co-recruiting additional neural resources to adopt increased memory demand difficulty in maintaining and manipulating TWM.

Effective connectivity and modulation of demand difficulty

The group-averaged DCM results (Fig. 5) showed effective connectivity within the left SI-dlPFC-PPC network during the delay period of Session 1 and the retrieval period of Session 2. The effective connectivity results showed how the ROIs in the SI and FP network influenced each other in the maintenance and manipulation processes of TWM. The dlPFC → PPC and dlPFC → SI connections, during the delay period, showed enhanced effective connectivity during the maintenance of information, whereas the PPC → dlPFC connection was suppressed. The dlPFC, the core of the central control network in the WM, controls and regulates attention and decides which information to maintain or manipulate[42–44]. However, the PPC integrates and transforms sensory representations[15]. These enhanced connections show that the dlPFC strengthens its communication with regions, including the PPC and SI, to manage memory maintenance and manipulation during the manipulation of memory information; while the PPC → dlPFC connection was significantly enhanced, providing evidence of PPC's active role in retrieving stored memory[45].

Modulatory results during the delay period (Fig. 5A.a) showed that the PPC → SI connection was significantly positively modulated in the high task demand (ORDER) compared with the low task demand (REPEAT). This indicated enhanced communication from the PPC to the SI in response to an increased memory capacity demand. A previous study on tactile short-term memory[36] showed that top-down regulation occurs in the connections between the prefrontal and parietal regions and the SI. This regulation might depend on information stored in the SI during the encoding period[5]. Excitatory modulation was observed exclusively when sensory information was temporarily maintained under high-demand conditions but not under low-demand conditions. These results show that increased memory demand specifically triggers enhanced neural activity to support the retention of sensory information, highlighting a demand-dependent mechanism that mobilizes additional resources when required by an overly high demand.

Furthermore, the PPC is closely involved in processing tactile spatial information by receiving inputs from the somatosensory cortex[46,47] and interacting extensively with frontal regions, including the inferior frontal gyrus and prefrontal cortex[14]. Since the tactile stimuli were identical in the high- and low-demand conditions, the differences in the SI and PPC pathways likely varied in memory demands, leading to the observed discrepancies in activating the intensity of WM maintenance.

We also observed that during the retrieval of tactile memory, in response to the higher task demand, the connection in the PPC → dlPFC and dlPFC → SI pathways were excitatory modulated. When manipulating temporary tactile information, its influence on the SI is intensified by the dlPFC to enhance memory retrieval under high demands. This enhanced modulation likely supports the processing of complex sensory information[47]. However, extensive information exchange from the dlPFC to PPC was reduced, which was associated with less significant modulation. Therefore, we speculated that the dlPFC → SI pathway experiences a significant increase in connectivity modulated by high task demand during manipulating information. In this case, the SI likely responds to retrieval instructions from the dlPFC using the tactile information temporarily stored during the early TWM period. This hypothesis is consistent with the sensory recruitment account[11,24], supporting the efficient involvement and modulation of sensory cortices during WM processes.

Therefore, the effective connectivity results show dynamic communication in the left SI-dlPFC-PPC network in modulating TWM with increasing task demand. Complex connectivity shows evidence that the task demand modulates the strength of neural contributions during tactile TWM[48], resulting in distinct interaction intensities. Notably, the SI might be a critical relay station for stimuli, coordinating with the FP regions, and is mobilized under higher-demand conditions, where effective sensory recruitment and information transfer are required.

Limitations

This study provides novel insights into TWM processing, yet several methodological limitations should be acknowledged. First, the retro-cues could introduce post-stimulus attentional reallocation confounds[40,49], and may not fully dissociate attentional modulation from TWM maintenance. A standard delayed match-to-sample (DMS) task[50] can properly isolate TWM-specific processes. Second, despite participants being instructed to avoid subvocalization, the prolonged maintenance intervals might have facilitated verbal recoding of stimuli[51]. To further explore this issue, an additional ERA analysis of the core Wernicke's area showed no significant difference between high- and low-demand tasks. In future work, the frequency-based stimuli (graded vibrations) or left-hand stimulation could better prevent verbal recoding. Third, due to constraints of the MRI hardware and total feasible scan time, we limited the number of trials to 15 per condition. Although our post hoc analysis in SI suggests that the current GLM design achieves power > 0.9, such retrospective power calculations are often viewed by researchers as potentially circular and should therefore be interpreted with caution. Finally, the ORDER and REPEAT tasks may rely on qualitatively different representations (sequence versus identity) raising the possibility that additional representational systems were recruited across conditions. Our fMRI results cannot totally rule out the involvement of language-related regions. Combining multivariate decoding and connectivity analyses in future studies would help to more clearly dissociate representational and non-representational components within brain areas.

Conclusion

This study provides further evidence for task demand modulation of the left SI and FP connectivity in maintaining and manipulating various processes of TWM. First, in maintaining and manipulating sensory information, the signal of the left SI shows greater activity in the high-demand condition. Also, the high-demand condition presents the significant functional connection between the left SI and FP regions. In the effective connectivity, the high-demand condition positively modulates the PPC → SI pathway during memory maintenance and the PPC → dlPFC and dlPFC → SI pathways during memory manipulation. These findings show how the left SI-dlPFC-

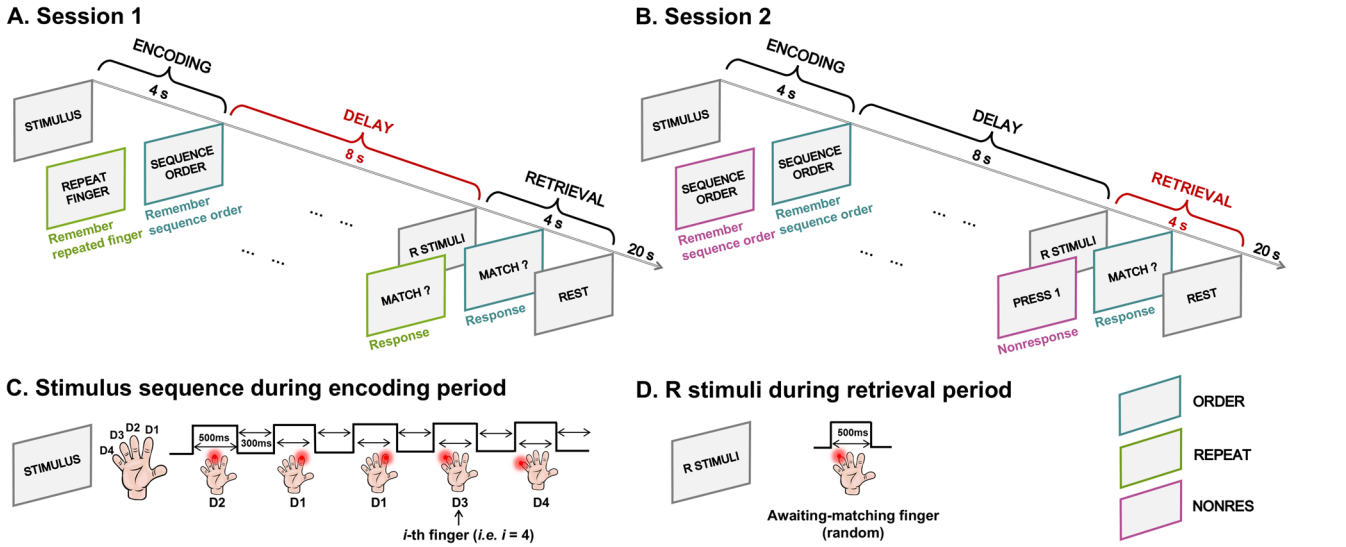

Fig. 6 | Experimental paradigm. Each trial comprised a 16-s task block, followed by a 20-s rest block. There was a rest (20 s) after each task trial. Notably, all conditions included five tactile stimuli during the encoding period (4 s). **A** Trial structure of Session 1. The primary difference between conditions was the delay period (8 s), where participants remembered the 'sequence order' (ORDER) and the 'repeat finger' (REPEAT). The retrieval period (4 s) involved determining if the R STIMULI matched the i-th finger (ORDER) or the repeated finger (REPEAT). **B** Trial structure of Session 2. The ORDER and NONRES conditions involved remembering the sequence order during the delay period; however, the primary difference was in the retrieval period. The ORDER condition matched Session 1, whereas the NONRES condition required no response, and the participants had to only press button 1. **C** During the encoding period, five random stimuli of four fingers were presented, and the i-th finger was queried in the ORDER and NONRES conditions. **D** During the retrieval period, a random awaiting-matching finger (R STIMULI) was presented for comparison. All elements were created by the authors using Microsoft PowerPoint (Microsoft Corporation).

PPC network dynamically distributes resources to handle increased memory demand. Consequently, these results emphasize the coordinated role of the SI with the FP regions during TWM, further confirming that the left SI may function as a central hub for information exchange to maintain and manipulate stimulus representations with increasing task demand.

Methods

Participants

In this experiment, 28 participants (mean age ± SD: 24.9 ± 1.8; 15 females, 13 males; education years: 15; all right-handed) completed the fMRI scanning. A post hoc power analysis was conducted using GPower v.3.1 to evaluate the achieved statistical power of the behavioral results[52,53]. Based on the observed mean accuracies (0.84 for the ORDER condition and 0.94 for the REPEAT condition) and standard deviations, the calculated effect size was Cohen's d = 1.32. Using a paired t-test with α = 0.05 and a total sample size of 28, the results indicated an achieved power of approximately 1.0. These suggest that the number of participants provided sufficient statistical power for detecting behavioral differences between conditions. A licensed neurologist supervised the administration of a comprehensive neuropsychological test battery to assess participants' cognitive function, including: Mini-Mental State Examination (MMSE), Montreal Cognitive Assessment-Basic (MoCA-B), Subjective Cognitive Decline Questionnaire (SCD-Q24), Auditory Verbal Learning Test (AVLT), Trail Making Test (TMT), and Symbol Digit Modalities Test (SDMT). All participants were healthy and possessed cognitive ability. They were recruited from the Shenzhen Institute of Advanced Technology, Chinese Academy of Sciences. All participants were fully aware of the nature of the study and provided written informed consent. All participants were invited to familiarize themselves with the experimental procedure before the formal experiment. The participants received a fixed payment after completing the entire experiment. The ethics committee of The Shenzhen Institute of Advanced Technology, Chinese Academy of Sciences, approved this study's experimental procedures. This study was conducted according to the Declaration of Helsinki. All ethical regulations relevant to human research participants were followed.

Experimental devices

A pneumatic stimulation system[27] was used to apply a tactile stimulus to the fingertips in the right hand. The pneumatic stimulation system had an air pump, a programmable logic controller (PLC), plastic pipes, and gloves with stimulation probes. Plastic pipes were used to connect the stimulation probes to the air pump, which was placed in the MRI operating room and did not interfere with the high magnetic fields. A personal computer in the MRI operating room was used to control the experimental setup. Notably, the signal generated by the computer is transmitted to the PLC, and a pressure stimulus is generated on an appropriate fingertip. Instructions for the experimental tasks were shown using E-Prime (version 3.0; Psychology Software Tools, Inc., Pittsburgh, PA, USA). They were projected from a shielded projector onto a screen mounted in the bore of the MRI scanner. The image from the projector was reflected in the participant's visual field using a head-coil-mounted mirror. A fiber optic button system (BrainLogic, Psychology Software Tools) was used to record all responses, including two buttons held by participants.

Experimental procedure

Each participant completed two 18 min sessions: Session 1 (Fig. 6A) included the ORDER and REPEAT conditions, while Session 2 (Fig. 6B) included the ORDER and NONRES conditions. Each condition had 15 trials, and each trial consisted of a 16 s task block (encompassing encoding, delay, and retrieval phases), followed by a 20 s rest block with a fixation point.

An air-puff stimulation generated by a pneumatic stimulation system was used five times for 500 ms with an inter-stimulus interval of 300 ms to four fingers (index, middle, ring, and little fingers) of the right hand during the 4-s encoding period (Fig. 6C). One finger was stimulated twice. That finger was referred to as the 'repeat finger,' while the others were stimulated once in a random order. Participants were required to memorize the entire stimulus sequence.

A cue was presented on the screen to show that relevant information should be retained during the 8 s delay period. In the ORDER and NONRES conditions, the cue instructed participants to remember the full stimulus

sequence, whereas the cue directed them to focus on recalling the repeated finger in the REPEAT condition.

In the 4-s retrieval period (Fig. 6D), a randomly selected 'question finger' was stimulated, followed by a question on the screen. In the ORDER condition, the question asked, "Is the question finger the same as the i-th finger?" while the question asked in the REPEAT condition was, "Is the question finger the repeat finger?" Participants responded by pressing button 1 for 'yes' and button 2 for 'no.' In the NONRES condition, the screen displayed "Press button 1," requiring participants to press the designated button without undergoing any memory recall.

The difficulty levels were manipulated during the delay and retrieval periods. In Session 1, the ORDER represented a high task demand, which required maintaining and recalling more stimulus details, while the REPEAT was a lower one owing to its single memory information. In Session 2, the ORDER remained the most demanding in terms of manipulation, necessitating the active retrieval of sequential information, whereas the NONRES was the least challenging, as no recall was required. Notably, fMRI and behavioral data were simultaneously recorded. It made sure that the differences in tasks would lead to significant differences in performance and brain activity.

Imaging data acquisition and preprocessing

A Siemens MAGNETOM Prisma 3 T MRI scanner (Siemens, Erlangen, Germany) with a 32-channel RF coil (Nova Medical, Wilmington, MA, USA) was used to acquire all fMRI data to measure BOLD signals at the Shenzhen Institute of Advanced Technology, Chinese Academy of Sciences. Functional data were collected using the echo-planar imaging sequence with an interleaved slice acquisition order (repetition time [TR]/echo time [TE] = 2000/30 ms; field of view [FOV] = 220 mm; matrix size = 64 × 64; flip angle = 90°; slice thickness = 3.4 mm with a 0.68 mm gap; 33 slices). Each fMRI had a single task session lasting 18 min. The first three volumes of each task session were discarded to eliminate magnetic saturation effects, resulting in 540 usable volumes. A 3D T1-weighted magnetization-prepared rapid acquisition gradient echo sequence was used (TR/TE = 2530/2.96 ms; FOV = 256 mm; matrix size = 256 × 256; flip angle = 7°; slice thickness = 1 mm with a 0.5 mm gap; 192 sagittal slices) to acquire high-resolution images of each participant's brain for anatomical reference, functional data registration, and normalization to a standard T1 template (Montreal Neurological Institute, MNI, CA, USA). The total acquisition time for the structural scan was 6 min.

The Statistical Parametric Mapping software package (SPM12, Institute for Neurology, University College London, UK) was used to conduct data analysis. To correct for head-motion artifacts, images were spatially realigned to the first volume of the first run. And then resliced to account for geometrical distortions, using deformation field maps for improved accuracy. Then the functional data underwent slice-timing correction for adjustments in temporal differences in slice acquisition, and any remaining motion artifacts were mitigated using wavelet despiking[28,54]. Subsequently, the EPI images were co-registered to the participants' corresponding T1-weighted structural images for precise anatomical alignment[55]. The co-registered images were then normalized to the standard MNI (Montreal Neurological Institute) space using the unified segmentation approach ensuring consistency across participants[56]. These normalized images were interpolated using voxel size of $2 \times 2 \times 2$ mm^3. Finally, spatial smoothing was applied using an 8 mm full-width-at-half-maximum Gaussian kernel.

The whole-brain analysis

Statistical analyses were conducted using a standard general linear model (GLM) approach with SPM12. First, we excluded incorrect trials. The GLM regressors for the encoding, delay, and retrieval phases of all correct trials across the ORDER, REPEAT, and NONRES conditions in both sessions were included in the first-level models. However, co-activation was computed across all conditions in the second-level analysis during the encoding phase (ORDER ∩ REPEAT ∩ NONRES). For the delay period, the differential and conjunctive activations between ORDER and REPEAT were compared in Session 1. However, differential activation and co-activation during retrieval were computed for the ORDER and NONRES conditions in Session 2.

We used a full-factorial design option to specify a second-level design, including one subject factor and three first-level baseline contrasts corresponding to the ORDER, REPEAT, and NONRES conditions. Furthermore, a within-subject one-way analysis of variance (ANOVA) was used to compare the contrasts in each session to assess group-level activations. Notably, all brain activations in this study showed a voxel-level threshold of $p < 0.05$, with FWE correction[33,57]. Threshold statistical parametric maps were rendered on a standard three-dimensional brain template using SPM12. Furthermore, all reported coordinates corresponded to the MNI space, and all results were inclusively masked using the search mask.

To directly observe the dynamic changes of the left SI throughout the entire TWM process, we performed event-related average (ERA) curves (Fig. 3, Supplementary Data 2). We identified the peak T-value within the significant activation cluster of the left SI in the ORDER > REPEAT contrast during the delay phase of the GLM and used this peak (the left SI: x = −44, y = −32, z = 46) as the VOI coordinate. For each condition of each participant, an 8 mm-radius spherical VOI was extracted around this peak. BOLD signal values were extracted for the VOI, and the resulting time series were aligned to trial onsets at 2 s intervals. BOLD signals for each trial, including both task and baseline epochs, were averaged across trials to obtain condition-specific mean activation levels. Moreover, the mean baseline BOLD signal B_{con}^{-} was calculated by averaging signal during baseline time points across all conditions in each session. The baseline time points included the rest time points (from 26 s to 36 s in one trail). Afterwards, we statistically analyze the event-related average under high- and low-demand conditions across the two sessions for 28 participants, along with the 95% confidence intervals. The BOLD signals for the VOI at time point t was transformed to S_t' as follows, to yield values interpretable as percentage signal change[19]:

$$S_t' = \frac{S_t - B_{con}}{B_{con}} \times 100$$

The psychophysiological interaction analysis

Implemented in SPM12, the PPI analysis is a method for investigating the task-specific correlations of time series of VOIs in brain regions[20,58]. Specifically, PPI identifies voxel activity that demonstrates a significant correlation in a seed ROI with other related ROIs in a specific psychological context, such as the ORDER, REPEAT and NONRES conditions used in the present experiment.

For each individual, VOIs were extracted from peak coordinates of the left SI (x = −44, y = −32, z = 46) and identified in the ORDER > REPEAT contrast during the delay period and the ORDER > NONRES contrast during the retrieval period, at an uncorrected threshold $p < 0.001$, adjusted for F contrast. The VOIs were extracted from a sphere with a radius of 8 mm around the local maxima. The design matrix of the PPI included three main regressors[59]: physiological variables that represented the time series from the seed ROI, psychological variables that represented the conditions (ORDER, REPEAT, and NONRES), and PPI variables that represented the functional connections between the seed ROI and other regions. In the first-level GLMs, PPI variables were built as regressors of interest, whereas physiological and psychological variables were regressors of no interest. Fisher's z-transformation was used to transform the resulting contrast into a z-score for the subsequent group-level analysis. Furthermore, different contrasts of functional connectivity between the SI and FP regions were analyzed separately in the ORDER > REPEAT contrast of Session 1 and ORDER > NONRES contrast of Session 2.

The DCM analysis

In this study, DCM was used to analyze the strength and modulation of conditions on effective connectivity among ROIs. Specifically, DCM can be used to examine input-state-output neural states across a network of brain

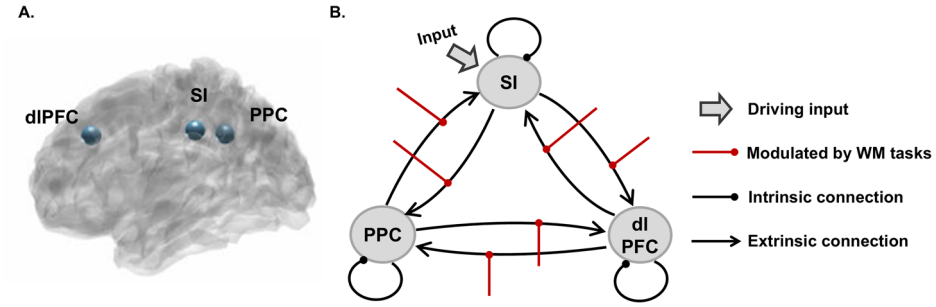

Fig. 7 | The SI–dlPFC–PPC effective connectivity framework. A Locations of ROIs (the left SI, PPC, and dlPFC) when building DCMs. **B** Network structure in DCMs, including a driving input from SI, connections modulated by WM tasks (ORDER/REPEAT/NONRES), and intrinsic connections and extrinsic connections among ROIs (the SI, dlPFC and PPC).

regions containing three distinct types of parameters[21]: driving input parameters demonstrating how brain regions respond to sensory stimuli (matrix C), intrinsic and extrinsic parameters characterizing the effective connectivity among regions (matrix A), and modulatory parameters describing changes modulated by experimental conditions (matrix B). The left SI, dlPFC, and PPC were selected as ROIs for constructing the DCM models based on their strong involvement in handling high tactile task demand[10] and significant activation at the whole-brain level during TWM (Table 2; Fig. 2). PPI analysis revealed functional connectivity between the seed ROI and other ROIs[60]; however, the DCM analysis focused on the modulatory effects of task demand on the interactions between these regions.

Each individual's VOI was surrounded with 8 mm eigenvariate spheres by the peak MNI coordinates, including the SI (x = −44, y = −32, z = 46), dlPFC (x = −20, y = 48, z = 36), and PPC (x = −26, y = −50, z = 38). Every VOI was set separately from the delay period of Session 1 (ORDER and REPEAT conditions) and the retrieval period of Session 2 (ORDER and NONRES conditions), both at an uncorrected threshold of $p < 0.001$, adjusted for the F contrast. Figure 7A shows the location of the ROIs.

Generally, the direct influence of experimental stimuli on specific regions can be modeled as a driving input[58,61]. Hypothetically, the tactile sensory input was primarily processed in the left SI. Intrinsic connections were treated as inhibitory self-connections in the ROIs, whereas extrinsic connections were bidirectional. Modulatory connections, influenced by task demand, covered all possible directional connections between ROIs. The DCMs for ORDER vs. REPEAT were computed during the delay period and ORDER vs. NONRES during retrieval, with 64 DCMs per participant. Figure 7B (Supplementary Data 3) shows the network structure of the DCMs, and model parameters were assessed using a one-state, bilinear, deterministic DCM.

At the group level, a PEB analysis was used to estimate the DCM parameters by combining individual-level DCMs with a group-level GLM to form an overall-level Bayesian framework[62]. Bayesian model averaging was conducted to statistically compare the model parameters, yielding an average group of Ep across the entire model space, weighted by each model's Pp. Usually, connections with Pp > 0.95 were considered significant. Positive Ep values indicated excitatory connections, whereas negative values indicated inhibitory connections. The Ep and Pp values for matrices A, B, and C are reported for each condition in Sessions 1 and 2. Furthermore, the effective connection differences during the delay and retrieval periods using an uncorrected threshold of $p < 0.05$ were compared using a one-way ANOVA.

Statistics and reproducibility

All statistical tests used, the sample sizes, the number of replicates, and how replicates were defined are described in the corresponding methods.

Reporting summary

Further information on research design is available in the Nature Portfolio Reporting Summary linked to this article.

Data availability

The datasets generated during the current study are available from the corresponding author on reasonable request. The source data for the figures are available in the Supplementary Data files.

Code availability

All code is available in the following GitHub repository: https://github.com/Sunnder39/my-basic-BOLD-fMRI-codebase.

Received: 26 October 2024; Accepted: 13 January 2026;
Published online: 23 January 2026

References

1. Baddeley, A. Working memory. *Science* **255**, 556-559 (1992).
2. Service, E. The effect of word length on immediate serial recall depends on phonological complexity, not articulatory duration. *Q. J. Exp. Psychol. A Hum. Exp. Psychol.* **51A**, 283–304 (1998).
3. Bays, P. M., Catalao, R. F. & Husain, M. The precision of visual working memory is set by allocation of a shared resource. *J. Vis.* **9**, 7.1–11 (2009).
4. Nielsen, J. D. et al. Working Memory Modulation of Frontoparietal Network Connectivity in First-Episode Schizophrenia. *Cerebral Cortex* **27**, 3832–3841 (2017).
5. Zanto, T. P., Rubens, M. T., Thangavel, A. & Gazzaley, A. Causal role of the prefrontal cortex in top-down modulation of visual processing and working memory. *Nat. Neurosci.* **14**, 656–661 (2011).
6. Constantinidis, C. & Procyk, E. The primate working memory networks. *Cogn. Affect. Behav. Neurosci.* **4**, 444–465 (2004).
7. Badre, D. & Wagner, A. D. Selection, integration, and conflict monitoring; assessing the nature and generality of prefrontal cognitive control mechanisms. *Neuron* **41**, 473–487 (2004).
8. Romo, R., Hernández, A., Zainos, A. & Salinas, E. Somatosensory discrimination based on cortical microstimulation. *Nature* **392**, 387–390 (1998).
9. Salazar, R. F., Dotson, N. M., Bressler, S. L. & Gray, C. M. Content-specific fronto-parietal synchronization during visual working memory. *Science* **338**, 1097–1100 (2012).
10. Rottschy, C. et al. Modelling neural correlates of working memory: a coordinate-based meta-analysis. *NeuroImage* **60**, 830–846 (2012).
11. C. S. Adam, K., Rademaker, R. L. & Serences, J. T. Evidence for, and challenges to, sensory recruitment models of visual working memory, in *Visual memory*. 5-25 (Routledge, 2022).
12. Vogel, E. K., McCollough, A. W. & Machizawa, M. G. Neural measures reveal individual differences in controlling access to working memory. *Nature* **438**, 500–503 (2005).
13. Katus, T., Grubert, A. & Eimer, M. Electrophysiological evidence for a sensory recruitment model of somatosensory working memory. *Cereb. Cortex* **25**, 4697–4703 (2014).
14. Ma, L. et al. Working memory load modulation of parieto-frontal connections: evidence from dynamic causal modeling. *Hum. Brain Mapp.* **33**, 1850–1867 (2012).

15. Murray, J. D., Jaramillo, J. & Wang, X. J. Working memory and decision-making in a frontoparietal circuit model. *J. Neurosci. Off. J. Soc. Neurosci.* **37**, 12167–12186 (2017).
16. Dima, D., Jogia, J. & Frangou, S. Dynamic causal modeling of load-dependent modulation of effective connectivity within the verbal working memory network. *Hum. brain Mapp.* **35**, 3025–3035 (2014).
17. Pasternak, T. & Greenlee, M. W. Working memory in primate sensory systems. *Nat. Rev. Neurosci.* **6**, 97–107 (2005).
18. Astle, D. E., Summerfield, J., Griffin, I. & Nobre, A. C. Orienting attention to locations in mental representations. *Atten. Percept. Psychophys.* **74**, 146–162 (2012).
19. Finn, E. S., Huber, L., Jangraw, D. C., Molfese, P. J. & Bandettini, P. A. Layer-dependent activity in human prefrontal cortex during working memory. *Nat. Neurosci.* **22**, 1687–1695 (2019).
20. Friston, K. J. et al. Psychophysiological and modulatory interactions in neuroimaging. *NeuroImage* **6**, 218–229 (1997).
21. Friston, K. J. et al. Bayesian model reduction and empirical Bayes for group (DCM) studies. *NeuroImage* **128**, 413–431 (2016).
22. Friston, K. Causal modelling and brain connectivity in functional magnetic resonance imaging. *PLoS Biol.* **7**, e33 (2009).
23. Ma, W. J., Husain, M. & Bays, P. M. Changing concepts of working memory. *Nat. Neurosci.* **17**, 347–356 (2014).
24. Degutis, J. K. et al. Dynamic layer-specific processing in the prefrontal cortex during working memory. *Commun. Biol.* **7**, 1140 (2023).
25. Hernández, A., Zainos, A. & Romo, R. Temporal evolution of a decision-making process in medial premotor cortex. *Neuron* **33**, 959–972 (2002).
26. Romo, R. & Salinas, E. Flutter discrimination: neural codes, perception, memory and decision making. *Nat. Rev. Neurosci.* **4**, 203–218 (2003).
27. Jia, S. et al. Pneumatical-Mechanical. *Tactile Stimul. Device Somatotopic Mapp. Body Surf. fMRI* **52**, 1093–1101 (2020).
28. Friston, K. J., Williams, S., Howard, R., Frackowiak, R. S. & Turner, R. Movement-related effects in fMRI time-series. *Magn. Reson. Med.* **35**, 346–355 (1996).
29. Karadachka, K. et al. Structural connectivity of the multiple demand network in humans and comparison to the macaque brain. *Cerebral Cortex* **33**, 10959–10971 (2023).
30. Funahashi, S., Bruce, C. J. & Goldman-Rakic, P. S. Mnemonic coding of visual space in the monkey's dorsolateral prefrontal cortex. *J. Neurophysiol.* **61**, 331–349 (1989).
31. Romo, R., Brody, C. D., Hernández, A. & Lemus, L. Neuronal correlates of parametric working memory in the prefrontal cortex. *Nature* **399**, 470–473 (1999).
32. Lloyd, D. M., Shore, D. I., Spence, C. & Calvert, G. A. Multisensory representation of limb position in human premotor cortex. *Nat. Neurosci.* **6**, 17–18 (2003).
33. Benjamini, Y. & Hochberg, Y. Controlling the false discovery rate: a practical and powerful approach to multiple testing. *Behav. Brain Res.* **57**, 289-300 (1995).
34. Spitzer, B., Gloel, M., Schmidt, T. T. & Blankenburg, F. Working memory coding of analog stimulus properties in the human prefrontal cortex. *Cerebral Cortex* **24**, 2229–2236 (2014).
35. Romo, R. & Salinas, E. Touch and go: decision-making mechanisms in somatosensation. *Annu. Rev. Neurosci.* **24**, 107–137 (2001).
36. Zhao, D., Zhou, Y. D., Bodner, M. & Ku, Y. The causal role of the prefrontal cortex and somatosensory cortex in tactile working memory. *Cerebral Cortex* **28**, 3468–3477 (2018).
37. Condylis, C. et al. Context-dependent sensory processing across primary and secondary somatosensory cortex. *Neuron* **106**, 515–525 (2020).
38. Laing, J. M. & Hampstead, B. M. Cognitive Compensatory Mechanisms, in *Encyclopedia of Gerontology and Population Aging*. (eds. D. Gu & M. E. Dupre) 1057-1061 (Springer International Publishing, 2021).
39. Schmidt, T. T. & Blankenburg, F. Brain regions that retain the spatial layout of tactile stimuli during working memory – A 'tactospatial sketchpad'? *NeuroImage* **178**, 531–539 (2018).
40. Rizza, A. et al. Working memory maintenance of visual and auditory spatial information relies on supramodal neural codes in the dorsal frontoparietal cortex. *Brain Sci.* **14**, 14020143 (2024).
41. Savini, N., Brunetti, M., Babiloni, C. & Ferretti, A. Working memory of somatosensory stimuli: an fMRI study. *Int. J. Psychophysiol. Off. J. Int. Organ. Psychophysiol.* **86**, 220–228 (2012).
42. Zhou, H. X. et al. Rumination and the default mode network: meta-analysis of brain imaging studies and implications for depression. *NeuroImage* **206**, 116287 (2020).
43. D'Esposito, M. et al. The neural basis of the central executive system of working memory. *Nature* **378**, 279–281 (1995).
44. Hagler, D. J. Jr. & Sereno, M. I. Spatial maps in frontal and prefrontal cortex. *NeuroImage* **29**, 567–577 (2006).
45. Christophel, T. B., Klink, P. C., Spitzer, B., Roelfsema, P. R. & Haynes, J. D. The distributed nature of working memory. *Trends Cogn. Sci.* **21**, 111–124 (2017).
46. Ku, Y. et al. Sequential roles of primary somatosensory cortex and posterior parietal cortex in tactile-visual cross-modal working memory: a single-pulse transcranial magnetic stimulation (spTMS) study. *Brain Stimul.* **8**, 88–91 (2015).
47. Ku, Y., Zhao, D., Bodner, M. & Zhou, Y. D. Cooperative processing in primary somatosensory cortex and posterior parietal cortex during tactile working memory. *Eur. J. Neurosci.* **42**, 1905–1911 (2015).
48. Brockhoff, L., Schindler, S., Bruchmann, M. & Straube, T. Effects of perceptual and working memory load on brain responses to task-irrelevant stimuli: review and implications for future research. *Neurosci. Biobehav. Rev.* **135**, 104580 (2022).
49. Souza, A. S. & Oberauer, K. In search of the focus of attention in working memory: 13 years of the retro-cue effect. *Atten. Percept. Psychophys.* **78**, 1839–1860 (2016).
50. Ohara, S., Lenz, F. & Zhou, Y. D. Sequential neural processes of tactile–visual crossmodal working memory. *Neuroscience* **139**, 299–309 (2006).
51. Berlin, D. F. Tactile discrimination, response mode, and interhemispheric communication by learning disabled children. *Percept. Mot. Skills* **72**, 504–506 (1991).
52. Faul, F., Erdfelder, E., Lang, A. G. & Buchner, A. G. Power 3: a flexible statistical power analysis program for the social, behavioral, and biomedical sciences. *Behav. Res. Methods* **39**, 175–191 (2007).
53. Zhang, Z. et al. Salient properties in bimanual haptic volume perception: influence of object shape, finger pair, and schizotypal personality traits. *IEEE Trans. Haptics* **14**, 816–824 (2021).
54. Patel, A. X. et al. A wavelet method for modeling and despiking motion artifacts from resting-state fMRI time series. *NeuroImage* **95**, 287–304 (2014).
55. Pan, M., Tang, J. & Xiong, Q. Medical image registration using fuzzy theory. *Comp. Methods Biomech. Biomed. Eng.* **15**, 721–734 (2012).
56. Ashburner, J. & Friston, K. J. Unified segmentation. *NeuroImage* **26**, 839–851 (2005).
57. Zhang, H. et al. Interaction between memory load and experimental design on brain connectivity and network topology. *Neurosci. Bull.* **39**, 631–644 (2023).
58. Cisler, J. M., Bush, K. & Steele, J. S. A comparison of statistical methods for detecting context-modulated functional connectivity in fMRI. *NeuroImage* **84**, 1042–1052 (2014).
59. O'Reilly, J. X., Woolrich, M. W., Behrens, T. E., Smith, S. M. & Johansen-Berg, H. Tools of the trade: psychophysiological interactions and functional connectivity. *Soc. Cogn. Affect. Neurosci.* **7**, 604–609 (2012).
60. Kahan, J. & Foltynie, T. Understanding DCM: ten simple rules for the clinician. *NeuroImage* **83**, 542–549 (2013).

61. Sun, D. et al. The role of occipitotemporal network for speed-reading: an fMRI study. *Neurosci. Bull.* **40**, 1261–1273 (2024).
62. Zeidman, P. et al. A guide to group effective connectivity analysis, part 2: second level analysis with PEB. *NeuroImage* **200**, 12–25 (2019).

Acknowledgements

Data of this work are provided by Shenzhen Institute of Advanced Technology, Chinese Academy of Sciences. Funding: the Japan Society for the Promotion of Science (25K10812), Key Laboratory for Magnetic Resonance and Multimodality Imaging of Guangdong Province (2020B1212060051), Shenzhen Basic Research Program (JCYJ20241202124859016), Guang Dong Basic and Applied Basic Research Foundation (2023A1515012929).

Author contributions

Z.Z. and L.W. supervised the study throughout all stages, guided the conceptual framework and manuscript writing, and provided funding support. D.S., as the first author, was responsible for data acquisition, data analysis, and the drafting and revisions of the main manuscript. J.Z. provided the experimental equipment, technical support, and guidance on multiple manuscript modification. S.F. assisted with data acquisition and contributed to multiple manuscript modifications. J.L. provided technical support for experimental equipment. Q.L. assisted with data acquisition. S.F. and T.M. supervised revisions of the manuscript and responses to reviewer comments. J.W. provided guidance on the conceptualization and initial manuscript.

Competing interests

The authors declare no competing interests.

Additional information

Supplementary information The online version contains supplementary material available at https://doi.org/10.1038/s42003-026-09586-y.

Correspondence and requests for materials should be addressed to Luyao Wang or Zhilin Zhang.

Peer review information *Communications Biology* thanks Valerio Santangelo and the other, anonymous, reviewer(s) for their contribution to the peer review of this work. Primary Handling Editors: Michel Thiebaut de Schotten and Jasmine Pan.